JOURNAL OF MATERIALS SCIENCE **39** (2004) 1639– 1646

Deposition of thermal barrier coatings using the solution precursor plasma spray process

LIANGDE XIE
Department of Metallurgy and Materials Engineering, Institute of Materials Science, University of Connecticut, Storrs, CT 06269-3136, USA

XINQING MA
Inframat Corporation, Farmington, CT 06032, USA

ERIC H. JORDAN*
Department of Mechanical Engineering, Institute of Materials Science, University of Connecticut, Storrs, CT 06269-3136, USA
E-mail: jordan@engr.uconn.edu

NITIN P. PADTURE
Department of Metallurgy and Materials Engineering, Institute of Materials Science, University of Connecticut, Storrs, CT 06269-3136, USA

DANNY T. XIAO
Inframat Corporation, Farmington, CT 06032, USA

MAURICE GELL
Department of Metallurgy and Materials Engineering, Institute of Materials Science, University of Connecticut, Storrs, CT 06269-3136, USA

The solution-precursor plasma-spray (SPPS) process is capable of producing highly durable thermal barrier coatings. In an effort to improve the understanding of the deposition mechanisms in this novel process, a series of specific experiments, where the substrate is held stationary and the plasma torch is programmed to scan a single pass across the substrate, were conducted and the resulting deposits were carefully characterized. In addition to the deposition mechanisms identified previously in the stationary torch experiments, the deposition mechanisms of two other types of deposits, thin film and fine spherical particles, were identified in this study. The melting of inflight formed 7YSZ particles and their rapid solidification to form ultra-fine splats on the substrate was found to be the dominant deposition mechanism. The characterization of actual SPPS coatings confirmed that the various coating-deposition mechanisms identified in the model experiments occur in concert during the actual coating process. Adherent deposits (ultra-fine splats, deposits from gel-like precursor and film formed via chemical vapor deposition), unmelted particles (spherical particles, deposits from non-decomposed precursor) and porosity were estimated to constitute ~65, ~19 and ~16 vol%, of the coating, respectively.

1. Introduction

Thermal barrier coatings (TBCs) have been widely used in aircraft and industrial gas turbines to protect metal components from high temperatures [1–5]. The two commercial processes used for the deposition of TBCs are air plasma spray (APS) and electron-beam physical-vapor deposition (EB-PVD). APS TBCs are low-cost and have low thermal conductivities, relative to EB-PVD TBCs, but are also less durable [1–5]. In the APS process, ceramic powder, usually ZrO_2-7 wt% Y_2O_3 (7YSZ), is injected into the high temperature, high velocity plasma jet. The powder is melted and propelled toward the substrate. Upon impact, the molten particles solidify and form "splats". The accumulation of splats results in the buildup of the ceramic coating. The splat boundaries contain planar porosity, which contribute to the low thermal conductivity, but also to the lower spallation life of APS TBCs compared to EB-PVD TBCs.

Several new processes for the deposition of TBCs are under development [6–10]. Among them, the solution precursor plasma spray (SPPS) method, which is potentially a low cost process, offers the prospect

*Author to whom all correspondence should be addressed.

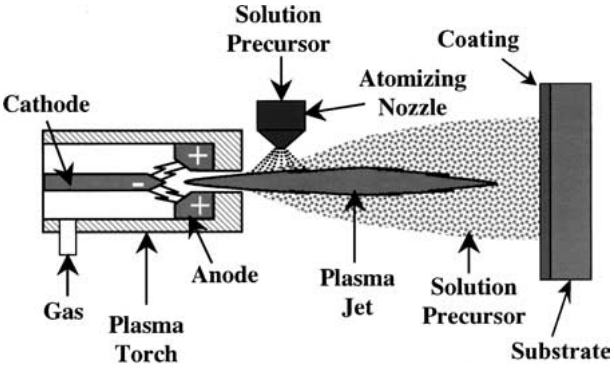

Figure 1 Schematic of the solution precursor plasma spray process.

of depositing highly durable TBCs that have low thermal conductivities [8]. In this process, an aqueous chemical precursor feedstock, containing yttrium and zirconium species, is injected into the plasma jet (Fig. 1). The precursor droplets undergo a series of physical changes and chemical reactions before being deposited on the substrate as a 7YSZ coating. A typical microstructure of a SPPS TBC is shown in Fig. 2. There are five main microstructural features [5, 8]: (i) dense region, (ii) unmelted particles, (iii) porosity, (iv) through-coating-thickness cracks, and (v) lack of large-scale "splat" boundaries that are always present in APS TBCs. The unmelted particles, the porosity, and the through-thickness cracks all impart strain tolerance to the TBC, while the porosity reduces the thermal conductivity. The lack of large-scale splat boundaries effectively toughens the TBC, making SPPS TBCs highly durable relative to APS TBCs [8, 11].

Extensive work aimed at understanding SPPS deposition mechanisms involved diagnostic experiments and model spray experiments [12–14]. Results from diagnostic experiments revealed that there are multiple pathways to SPPS coating formation [14]. Detailed characterization of the deposits collected in the stationary torch experiments identified the following coating-deposition mechanisms [13]: (a) Precursor droplets whose trajectory lies in the cold region (periphery) of the plasma jet inflate and rupture after landing on the substrate and integrate into the coating as flakes or irregular agglomerates after being covered over by subsequent deposits; (b) Precursor droplets injected into the core of the plasma jet experience evaporation and decomposition. The 7YSZ particles formed in the plasma melt during their flight in the plasma jet, and then impact onto the substrate at high velocity resulting in the formation of ultra-fine splats; (c) precursor droplets with most solvent evaporated during their flight in the plasma jet pyrolyze and crystallize on the substrate and form large "pancake"-like deposits.

Two additional deposition mechanisms were identified in this study, and the contribution of each deposition mechanism, identified previously and in this work, to the coating build-up was estimated. Based on the understanding gained from these model experiments, the processing-microstructure control required for specific coating applications is discussed.

2. Experimental procedures

2.1. SPPS deposition

Fig. 1 is a schematic illustration of the solution-precursor plasma-spray process, where an atomizer nozzle, attached to the plasma torch, injects solution-precursor mist into the plasma jet. The precursor used here is an aqueous solution containing zirconium and yttrium salts, to result in a 7YSZ ceramic coating [8, 12, 14]. All coatings reported here were deposited under nominally identical experimental conditions (plasma-spray parameters, solution-precursor flow rate and pressure, atomization parameters, solution concentration, and torch-substrate distance). Coatings were deposited

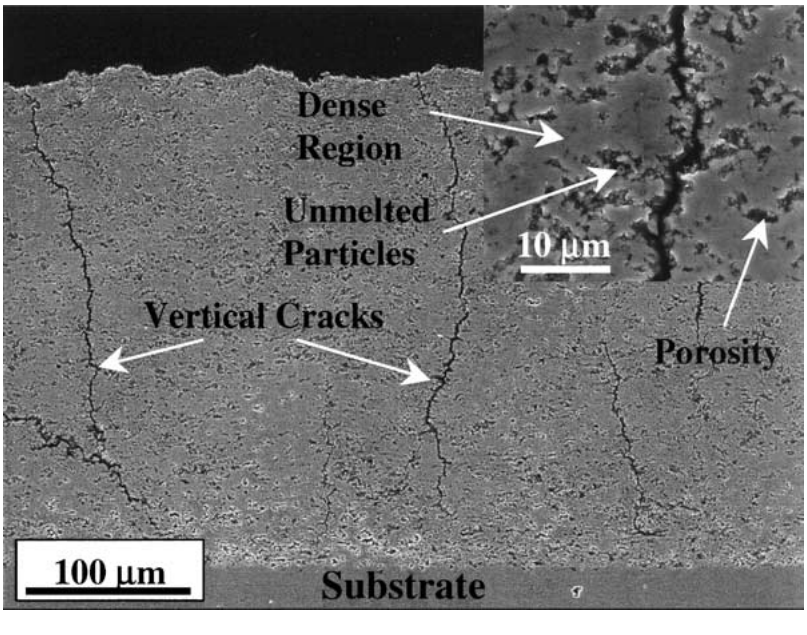

Figure 2 SEM micrograph of a polished cross-section view of a SPPS TBC showing vertical cracks. Higher-magnification inset shows the unmelted particles, porosity and no large "splat" boundaries.

on stainless steel substrates (plates 75 × 50 × 3 mm or disks 25 mm diameter, 3 mm thickness), surfaces of which were previously roughened by grit-blasting (Al_2O_3 grit of #320 mesh size) or polished metallographically to 1 μm finish.

The direct current (DC) plasma torch used here was the Metco 9 MB (Sulzer Metco, Westbury, NY), which was attached to a 6-axis robotic arm. The plasma power used was in the range 35 to 45 kW. Ar and H_2 were used as the primary and the secondary plasma gases, respectively, whereas N_2 was used as the solution-precursor atomizing gas. A resistance heater was used to preheat the substrate to a fixed high temperature, as measured using a thermocouple attached to the backside of the substrate.

In an effort to identify coating-deposition mechanisms other than those identified in the stationary torch experiments and determine the dominant deposition mechanism, two types of single-line scan-spray experiments were performed. In the first type, the plasma torch was programmed to scan one pass across the substrate at its maximum speed (~1200 mm/s), which is referred to as high-speed single-line experiment. In the second type, the plasma torch was programmed to scan a single pass across the substrate at the speed normally used for actual coating deposition (300–800 mm/s), which is referred to as normal-speed single-line experiment.

2.2. Characterization

The top surface of samples deposited in single-line scanning spray experiments were observed in a scanning electron microscope (SEM) (JSM6335F, Jeol, Japan) equipped with a field emission source. Deposits collected in normal-speed single-line experiments were also observed in an optical microscope (Macrophot^{TM}, Nikon, Japan).

Actual SPPS TBCs (300 μm) deposited using multi-pass rastering spray experiments (see details in [8, 14]) were also characterized to verify the occurrence of the identified coating-deposition mechanisms during the actual coating-deposition process and to estimate their contribution to the coating build-up. The fracture cross-section of the freestanding coating was obtained by notching the coating from the substrate with a diamond blade and then bending the coating. The exposed fracture surfaces were observed in the high-resolution SEM.

2.3. Image analysis

In an attempt to estimate the volume of dense region and unmelted particles in the actual coating, and hence the contribution of each coating-deposition mechanism to the coating build-up, the polished cross-section of the actual coating, prepared according to standard metallographic procedures, was ultrasonically cleaned to remove the unmelted particles, so that the dense region can be easily distinguished. After that, ten SEM pictures were taken and then analyzed using an image analyses system, microGOP 2000 (ContextVision, Linkoping, Sweden).

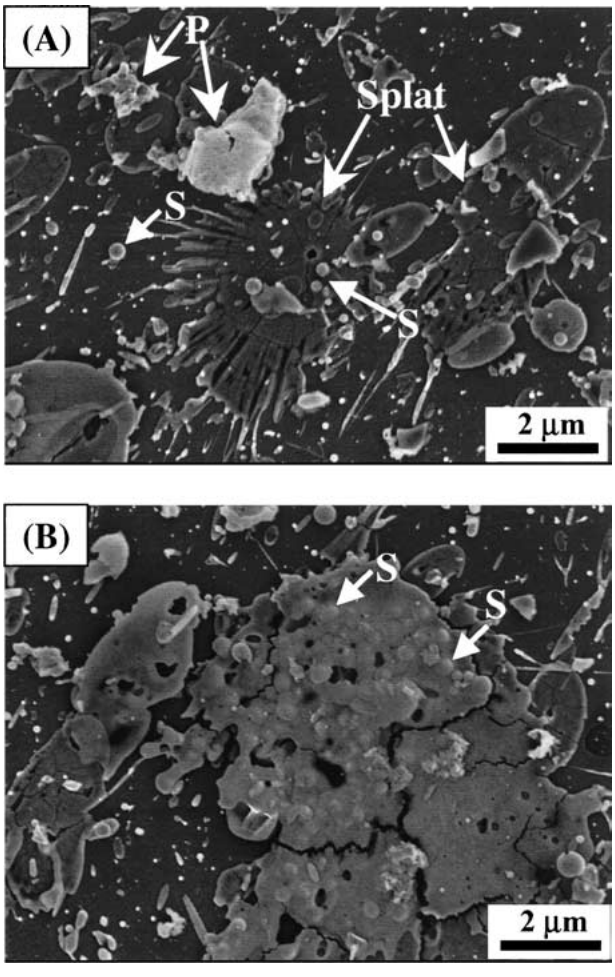

Figure 3 Deposits collected on room temperature substrate during high-speed single-line experiments, showing (A) the morphology of splat with many "fingers" from splashing and spherical particles landing on the substrate and splat (indicated with the arrow), (B) the spherical particles underneath the splat (indicated with the arrow).

3. Experimental results

3.1. High-speed single-line scan-spray experiments

3.1.1. Room-temperature substrate

Splats and deposits from non-decomposed precursor (*P*) previously observed in stationary torch experiments [13] are also present in the deposits collected on a room-temperature substrate during high-speed single-line scanning experiments (Fig. 3A). Some spheres (*S*) attach directly to the substrate or land on the top of the splats (Fig. 3A). Some others are buried under the splat (Fig. 3B). At the edge of the substrate (~40 mm from the axis of the plasma torch), corresponding to the region where the solution precursor droplet experiences little heating, deposits like Fig. 4A–C are present. Previous work indicates that these deposits result from precursor containing significant amount of solvent [13]. The deposit in Fig. 4A has a continuous and smooth surface. This morphology indicates that the precursor droplet reaches the substrate and spreads to a certain degree, then stays there and experiences little change. Many mudflat cracks are present in the deposits shown in Fig. 4B and C, which is the result of shrinkage due to evaporation of the solvent remaining in the deposits. The dimples in Fig. 4C (as judged under the microscope by adjusting the focus) indicate that solid spheres

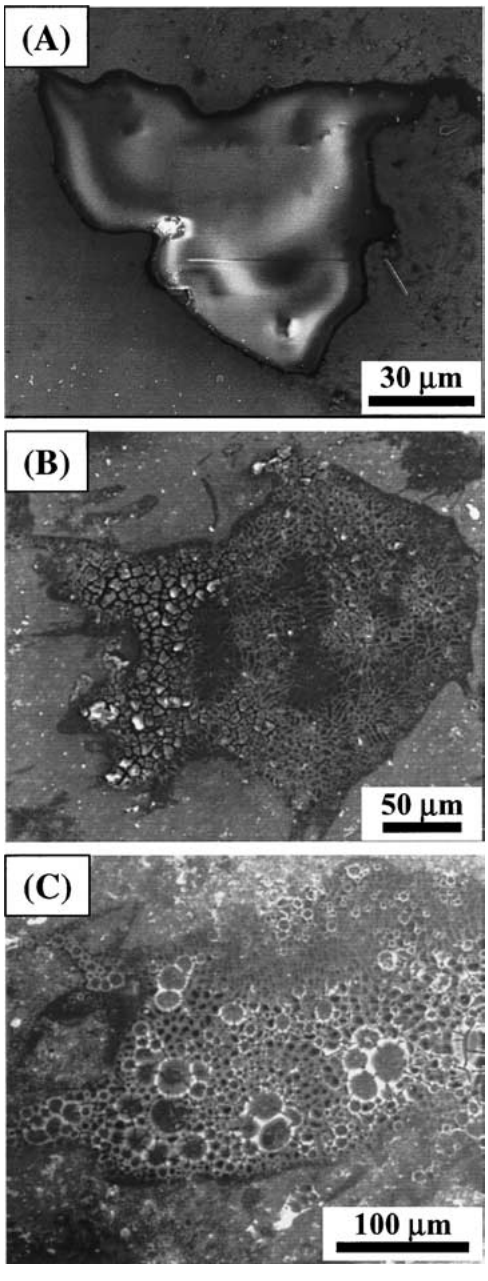

Figure 4 Deposits collected from the edge of the plasma jet (∼40 mm from the core), showing (A) the smooth surface, (B) "mud-flat" cracks on the surface, and (C) the dimples and "mud-flat" cracks on the surface.

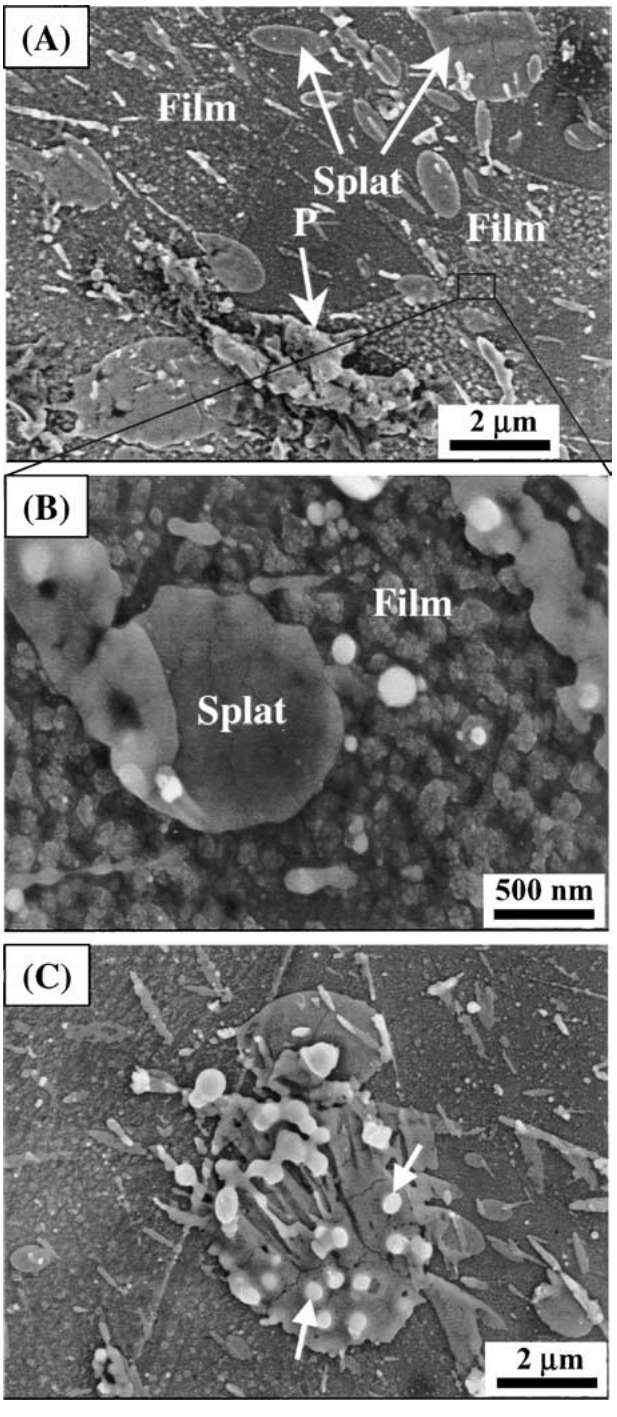

Figure 5 Deposits collected on 500°C substrate during high-speed single-line experiments, showing (A) the morphology of splat with no splashing and thin film, (B) details of the thin film, and (C) spherical particles cemented on the top of the splat (indicated with the arrow).

impacted on the deposits and bounced off, which suggests that these deposits can not retain the in-flight formed solid spheres on their surface.

3.1.2. High temperature substrate

Though similar splats and deposits from non-decomposed precursor (*P*), as previously described, are also present in the sample deposited on a high temperature substrate (500°C) during high-speed single-line experments (Fig. 5A), the morphology of the splats is more disk-like than that of splats collected on the room-temperature substrate (Fig. 3A). Splashing of the splats is greatly reduced on the high temperature substrate, consistent with the previously reported effects of substrate preheating in conventional plasma spray [15, 16].

Besides the previously observed deposits, a thin film with a ∼100 nm size feature is present, as shown in Fig. 5A, and more clearly in Fig. 5B. This thin film is absent in the deposits produced on the substrate at room temperature. The particulate morphology of the film is very similar to that of the coating produced using the electrostatic spray assisted vapor deposition (ESAVD) [9, 17], except that the size of the features in ESAVD coating are ∼100 times larger. In Fig. 5C, the spherical particles are on the top of the splat, and well bonded to the splat. These particles likely hit and stuck to the splat when it was solidifying.

3.2. Normal-speed single-line experiment

Fig. 6A is an optical photograph of the sample produced in the normal-speed single-line experiment. In

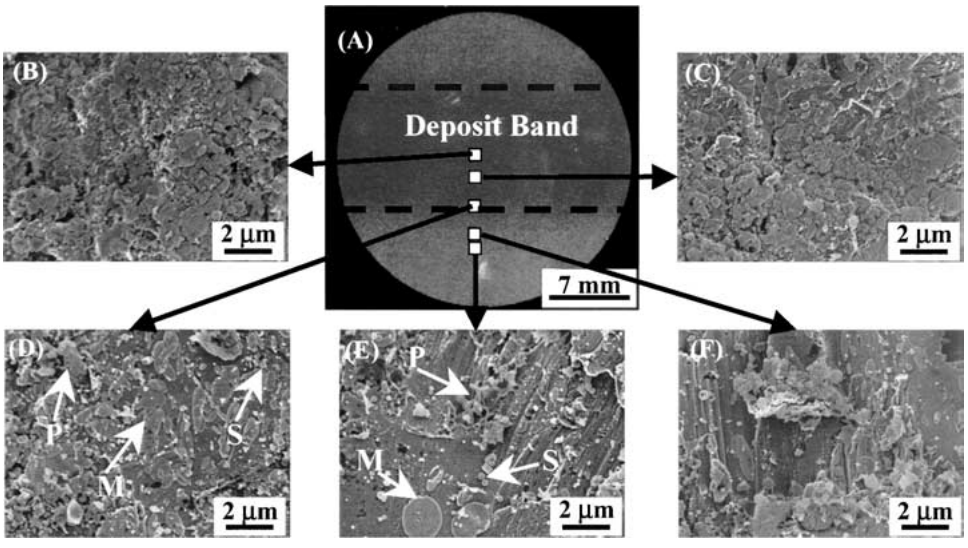

Figure 6 (A) Optical micrograph of the sample deposited in the normal-speed single-line experiments, (B)–(D) showing that most of the deposits within the deposit band are splats and the splat population decreases towards the deposit band edge, (E) and (F) showing the deposits are sparse outside the deposit band and most of them are from non-decomposed precursor.

this experiment, the substrate temperature (100–450°C) is the same as that used in the actual spraying. The change of deposit morphology as a function of the location across the path of plasma torch is shown in Fig. 6B–F. Within the deposit band, most of the deposits are splats (*M*) though some spherical particles (*S*) and irregular agglomerates (*P*) are also present at the edge of the deposit band (Fig. 6D). The population of deposits increases from the edge of the deposit band to the center where the substrate is fully covered with splats, as illustrated in Fig. 6B–D. Outside of the deposit band (Fig. 6E and F), there are spherical particles (*S*), a few splats (*M*) and residuals of the deposits from non-decomposed precursor (*P*).

3.3. Coatings

On the fracture surface of an actual SPPS TBC (Fig. 7A), the columnar structure of the splats (*M*) formed from rapid solidification of molten 7YSZ is observed, which confirms the finding from the stationary torch experiments [13] that melting and solidification occur in the SPPS process. In Fig. 7B and higher magnification picture Fig. 7C, equiaxed grains (*G*) are also observed, which may correspond to the deposit originating from the gel-like precursor [13]. Agglomerates and flakes (*P*) originating from non-decomposed precursor [13], and spherical particles (*S*) are also present in the fracture surface (Fig. 7B), which confirms that the deposits from non-decomposed precursor will be covered over by subsequent deposits, and thus be incorporated into the coating [13].

Fig. 8A and B are the polished cross section of the as-sprayed coating. It can be seen that most of the unmelted particles in the cross section (Fig. 8A) disappeared after ultrasonic cleaning (Fig. 8B). On the ultrasonically cleaned cross section, 10 pictures were taken randomly except that the vertical cracks were avoided. Results from image analysis indicate that the area of the matrix is ~65% and that of the cavities (porosity plus unmelted particles) are ~35% of the total area of the image, as shown in Fig. 9A.

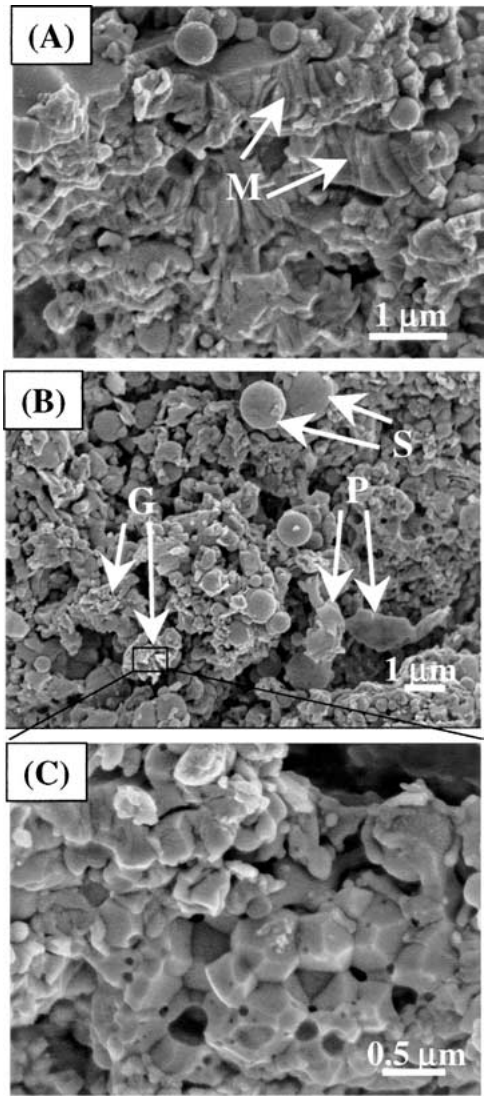

Figure 7 SEM micrographs of cross-section fracture surfaces of actual SPPS coatings: (A) "S" fine spherical particles, "P" flake-like deposits from wet-precursor, and "G" deposits from gel-like precursor, (B) higher magnification view of the "G" deposits showing equiaxed grain structure, and (C) "M" "splat" resulting from the melting and solidification of 7YSZ.

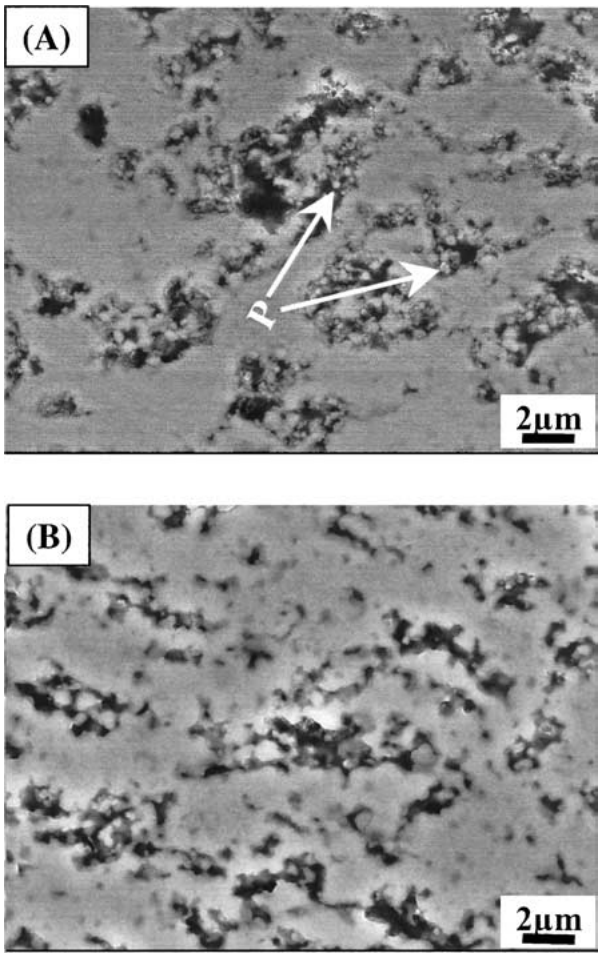

Figure 8 Polished cross section of the as-sprayed coating: (A) As prepared, (B) ultrasonically cleaned, showing that most of the unmelted particles in the as-prepared cross section disappeared after the ultrasonic cleaning.

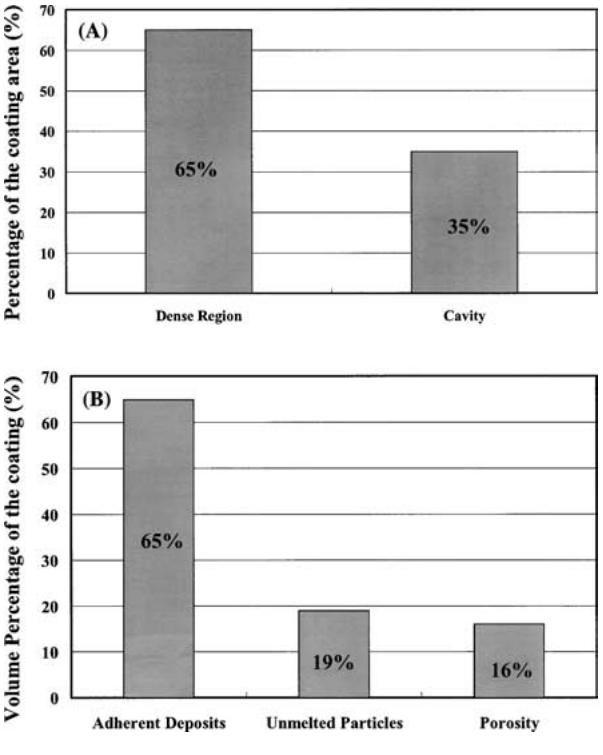

Figure 9 (A) The area percentage of the dense region and cavity in the ultrasonically cleaned polished cross-section of the coating, (B) estimated volume percentage of the adherent deposits, unmelted particles, and porosity in the coating.

4. Discussion

4.1. Deposition mechanisms

It is known that large temperature variations exist in the plasma jet [18]. To aid in discussion, the plasma jet can be divided into three regions as in Fig. 10A: (I) the periphery or cold region, (II) the moderately hot region, and (III) the core or hot region. Previous results from stationary torch experiments [13] reveal that the precursor droplets injected into the core of the plasma jet (region III in Fig. 10A) will experience melting and solidification and deposit on the substrate as ultra-fine splats (Fig. 10E), while the precursor droplets whose trajectory lies in the periphery of the plasma plume (region I in Fig. 10A) will inflate and rupture after landing on the substrate and integrate into the coating as flakes or irregular agglomerates (Fig. 10B) after being covered over by subsequent deposits. The thin film (Fig. 10C) and the fine spherical particles (Fig. 10D) are rarely observed in the deposits collected from either the core or the periphery of the plasma jet, therefore, they can be related to the precursor droplets injected into the moderately hot region of the plasma jet (region II in Fig. 10A). Here, we are going to discuss the deposition mechanism of the thin film and the fine spherical particles.

The regions marked as "film" in Fig. 5A and B have an appearance that suggests a vapor deposition mechanism. The film is not observed in the deposits collected from the core of the plasma jet where vaporization of 7YSZ ceramic is most likely to occur. This observation excludes physical vapor deposition as the deposition mechanism. The configuration of SPPS process is quite similar to that of the plasma assisted chemical vapor deposition (PACVD) process with liquid feedstock [19, 20] except that radio frequency plasma is used in PACVD, which results in lower plasma temperature. In addition, the morphology of the film in Fig. 5A and B resembles that of the TBCs deposited using electrostatic spray assisted vapor deposition (ESAVD), where heterogeneous chemical vapor deposition (CVD) is the deposition mechanism. Therefore, it is suggested that the film results from CVD occurring in the SPPS process. Furthermore, the substrate temperature in heterogeneous CVD process [21] must be higher than the decomposition temperature of the precursor (300–400°C for the precursor used here [14]), otherwise, adherent deposit will not form on the substrate. The absence of the film on the room temperature substrate supports this notion that the observed film is formed via CVD.

Solid spherical particles in the plasma jet may form by one of three routes: (i) the precursor droplets undergo decomposition in the plasma jet. The formed particles may crystallize or even sinter but not melt before reaching the substrate, (ii) 7YSZ particles formed from the decomposition of precursor melt and resolidify before reaching the substrate, which has been seen in thermal-fluids model of plasma sprayed Al_2O_3 deposits [22], and (iii) vaporized precursor decomposes and forms particles in the plasma. Regardless of how the spheres form, they rarely stay on the substrate by themselves. Deposits with significant amount of solvent do not trap spheres, but instead leave marks as the spheres bounce

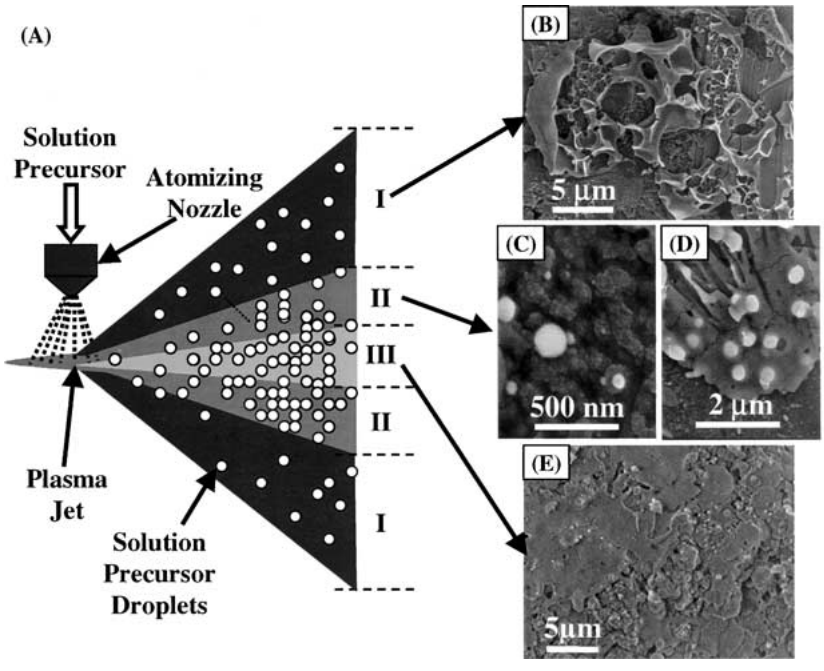

Figure 10 (A) Schematic of the temperature variation in the plasma jet, (I) the periphery or cold region, (II) the moderately hot region, and (III) the core or hot region; (B)–(E) the corresponding deposits formed from the precursor droplets injected into different regions of the plasma jet.

off (Fig. 4). However, spheres can be trapped by the molten splats as in Fig. 5C. It should be noted that not all spherical particles are solid when they land on the substrate. Some of them may be molten droplets without enough kinetic energy to form splats. These droplets can stay on the substrate by themselves (Fig. 3A). All of the trapped and attached spherical particles are integrated into the coating after being covered by subsequent deposits (e.g., Figs 3B, 7B and C).

There are striking similarities between the morphologies of the deposits collected in the stationary torch experiments [13], single-line scanning experiments (Figs 3 and 5) and the microstructural features observed in the actual coating (Fig. 7A to C). This remarkable resemblance indicates that the various deposition mechanisms, identified in the previous work [13] and this study, occur in concert during the deposition of actual SPPS coatings.

Films formed via CVD of the vaporized precursor are not observed in the actual coating. However, this cannot exclude the occurrence of CVD in the SPPS process. The much finer feature (∼100 nm) of the film relative to the size of other deposits (2–20 μm) and small thickness due to the low deposition rate of CVD process may make the film undetectable in the thick coating.

4.2. Coating build-up and optimization

All the processing parameters used in the normal-speed single-line scanning experiments are the same as those used to deposit actual coatings. It can be seen from Fig. 6A–F that most of the deposits within the deposit band are splats and the deposits outside of the deposit band are sparse. Therefore, it can be concluded that the dominant deposition mechanism in the deposition of TBCs using the SPPS process is the melting of the in-flight formed 7YSZ particles and their rapid solidification on the substrate. Similar coating deposition mechanism is operating in the APS process except that the feeding powder is synthesized prior to deposition. However, the diameter of the splats formed in the SPPS process is less than 2 μm [13], comparing with 20–50 μm of those formed in the APS process. The area of the splats is two orders of magnitude smaller than those in APS TBCs, which eliminates the large-scale splat boundaries in APS coatings, and thus improves the interface toughness between subsequent splats.

It's known from stationary torch experiments [13] that the dense region in the coating, as shown in Fig. 1, results from the precursor injected into the core of the plasma jet, while the unmelted particles in the coating correspond to the spherical particles and the non-decomposed precursor droplets landing on the substrate. This result is consistent with the findings from the previous multi-pass single-line scanning experiments [12] that the coating around the plasma torch axis has maximum density and the density of the coating decreases towards the edge of the plasma jet. Also, the unmelted particles in the coating can be greatly reduced by placing a ceramic window in front of the plasma jet to shield the precursor traveling in the outer region of the plasma jet from reaching the substrate [12].

From the fracture surface of the coating (Fig. 7A to C), it can be seen that most of the unmelted particles are just loosely attached to the adherent ones. Therefore, during metallographic preparation, especially after ultrasonic cleaning, most of the unmelted particles will be removed from the cross section. Accordingly, the relative volume of the dense region and that of the unmelted particles plus porosity can be estimated by the image analysis of the SEM pictures taken on the ultrasonically-cleaned polished cross section, which in turn gives an estimation of the relative contribution of adherent deposits and unmelted particles to the coating build-up. It should be noted that the contribution of

the adherent deposits would be slightly overstated due to the retaining of some unmelted particles in the cross section. Based on the result of image analysis (Fig. 9A), ∼65 vol% of the coating are adherent deposits, which consists mostly of splats, and also of deposits from gel-like precursor [13] and film formed via CVD. The unmelted particles plus the porosity constitute the other 35% of the volume of the produced coating. The porosity of the whole coating is around 16% [8]. Therefore, the unmelted particles, which include spherical particles and deposits resulting from non-decomposed precursor, consist ∼19 vol% of the coating (Fig. 9B).

With the afore-mentioned combination of adherent and unmelted particles, the coating microstructure as shown in Fig. 2 will be obtained. The coating with this microstructure exhibited superior durability compared to the conventional APS TBCs [11]. However, in some applications it is desirable to have a denser or a more porous coating. For example, the outer surface of a TBC needs to be erosion resistant and should be made denser, whilst a more porous coating is desirable on abradable seals. Based on the understanding of the deposition process, it is anticipated that the coating structure may be tailored by controlling the relative amount of adherent deposits and unmelted particles in the coating, which can be achieved by adjusting the liquid feed parameters, adopting axial liquid feeding system, using higher power plasma system, or shielding some precursor in the low temperature region of the plasma jet from reaching the substrate.

5. Conclusion

In addition to the deposition mechanisms identified previously in the stationary torch experiments [13], the deposition mechanism of two other types of deposits, thin film and fine spherical particles, were identified in this study. The thin film forms by CVD. The fine spherical particles are integrated into the coating after being trapped and covered over by subsequent deposits. The remarkable resemblance between the morphologies of the deposits collected in the stationary torch experiments, single-line scanning experiments and the microstructural features observed in the actual coatings indicates that the identified deposition mechanisms occur in concert during the deposition of actual SPPS coatings.

The melting of in-flight formed 7YSZ particles and their rapid solidification on the substrate was found to be the dominant deposition mechanism in the deposition of TBCs using the SPPS process. However, the ultra-fine splats thus produced are typically 3 orders of magnitude smaller in volume than those produced in the conventional APS process. Adherent deposits (splats, deposits from gel-like precursor and film formed via CVD), unmelted particles (spherical particles, deposits from non-decomposed precursor), and porosity were estimated to constitute ∼65, ∼19 and ∼16 vol% of the coating, respectively.

Acknowledgement

The authors thank Dr. T. Bhatia, Prof. B. M. Cetegen, and Mr. A. Ozturk, for fruitful discussions. This work is supported by U.S. Office of Naval Research (Grant no. N000014-02-1-0171), managed by Drs. Lawrence Kabacoff and Steven Fishman.

References

1. S. M. MEIER and D. K. GUPTA, *J. Eng. Gas Turbines Power* **116** (1994) 250.
2. S. MILLER, *Mater. World.* **4** (1996) 446.
3. R. A. MILLER, *J. Therm. Spray Technol.* **6** (1997) 35.
4. N. P. PADTURE, M. GELL and E. H. JORDAN, *Science* **296** (2002) 280.
5. D. W. PARKER, *Mat. Des.* **14** (1993) 345.
6. K. D. HARRIS, D. VICK, E. J. GONZALEZ, T. SMY, K. ROBBIE and M. J. BRETT, *Surf. Coat. Technol.* **138** (2001) 185.
7. D. D. HASS, A. J. SLIFKA and H. N. G. WADLEY, *Acta Mater.* **49** (2001) 973.
8. N. P. PADTURE, K. W. SCHLICHTING, T. BHATIA, A. OZTURK, B. CETEGEN, E. H. JORDAN, M. GELL, S. JIANG, T. D. XIAO, P. R. STRUTT, E. GARCIA, P. MIRANZO and M. I. OSENDI, *ibid.* **49** (2001) 2251.
9. J. D. VYAS and K. L. CHOY, *Mater. Sci. Eng.* A **277** (2000) 206.
10. B. PREAUCHAT and S. DRAWIN, *Surf. Coat. Technol.* **142–144** (2001) 835.
11. M. GELL, L. XIE, X. MA, E. H. JORDAN and N. P. PADTURE, *ibid.* (2003) in press.
12. L. XIE, X. MA, A. OZTURK, E. H. JORDAN, N. P. PADTURE, B. CETERGEN, D. XIAO and M. GELL, Submitted to *Surf. Coat. Technol.*, in press.
13. L. XIE, X. MA, E. H. JORDAN, N. P. PADTURE, D. XIAO and M. GELL, *Mater. Sci. Eng.* A **362** (2003) 204.
14. T. BHATIA, A. OZTURK, L. XIE, E. H. JORDAN, B. M. CETEGEN, M. GELL, X. MA and N. P. PADTURE, *J. Mater. Res.* **17** (2002) 2363.
15. S. SAMPATH, X. Y. JIANG, J. MATEJICEK, A. C. LEGER and A. VARDELLE, *Mater. Sci. Eng.* A **272** (1999) 181.
16. M. VARDELLE, A. VARDELLE, A. C. LEGER, P. FAUCHAIS and D. GOBIN, *J. Therm. Spray Technol.* **4** (1995) 50.
17. K. L. CHOY, *Mater. Sci. Eng.* C **16** (2001) 139.
18. S. SEMENOV and B. CETEGEN, *J. Therm. Spray Technol.* **10** (2000) 326.
19. N. YAMAGUCHI, T. HATTORI, K. TERASHIMA and T. YOSHIDA, *Thin Solid Films* **316** (1998) 185.
20. H. ZHU, Y. C. LAU and E. PFENDER, *J. Appl. Phys.* **69** (1991) 3404.
21. K. L. CHOY, *Progress in Mater. Sci.* **48** (2003) 57.
22. I. AHMED and T. L. BERGMAN, *J. Thermal Spray Technol.* **9** (2000) 215.

Received 7 May
and accepted 13 October 2003